Synsint Research Group

Available online at www.synsint.com

Synthesis and Sintering

ISSN 2564-0186 (Print), **ISSN** 2564-0194 (Online)

Review article

3D-printed calcium magnesium silicates: A mini-review

Aidin Doroudi [a,*], **Preeti Lata Mahapatra** [b], **Fatemeh Bakhshi** [a]

[a] *Polymer and Color Engineering Department, Amirkabir University of Technology, Tehran, Iran*
[b] *School of Nano Science and Technology, Indian Institute of Technology, Kharagpur, West Bengal-721302, India*

ABSTRACT

Calcium magnesium silicates (CMS) represent a class of minerals with diverse applications in fields ranging from geology to materials science. With the advent of additive manufacturing technologies, particularly 3D printing, novel opportunities have emerged for the synthesis and utilization of CMS-based materials. In this mini-review, we provide a thorough overview of recent advancements in the 3D printing of CMS compounds, including diopside (DPS), bredigite (BR), and akermanite (AKT). We discuss the synthesis methods, properties, and potential applications of 3D-printed CMS materials, with a focus on their role in biomedical applications. Furthermore, we highlight challenges and prospects in the field, emphasizing the importance of continued research and innovation in harnessing the full potential of 3D-printed CMS materials.

KEYWORDS

Calcium magnesium silicates
3D printing
Synthesis methods
Bioceramics
Additive manufacturing

OPEN ACCESS

1. Introduction

It's been a long time since bioactive glasses have been interested by a large number of researchers. Hench et al. [1] delved into biologically active bioglass for hard tissue regeneration in 1970 because of its bioactive nature, high compression strength, and ability to be fabricated using customized glass. Bioactive ceramics are osteoproductive and osteoconductive materials. Since these ceramics sinter quite well, they are perfect materials for making scaffolds. Because bioactive materials can promote the production of the apatite layer on their surface during in-vitro research, they have been exploited in the field of tissue engineering. Examples of these materials are calcium phosphates (CaPs) and silicate bioceramics (SBs). Accordingly, bioactive ceramics such as bredigite (BR), diopside (DPS), and akermanite (AKT) could be utilized to create scaffolds for bone tissue engineering (BTE) [2, 3].

Bioactive ceramics are utilized in biomedical applications including dental and orthopedic implants. Through a particular biological response at the materials' interface, bioactive materials directly interact with natural tissues. Like muscles, bones are living tissues that give the body structural support. Bone tissues that are injured or damaged as a result of diseases like osteoporosis are prone to fracture and become weak [4–6].

By depositing apatite, bioactive ceramics can restore several types of bone defects. Hard tissue engineering researchers are focusing their research on bioactive materials as a potential replacement for the commercially available polymeric and metallic biomaterials [3]. Meanwhile, SBs are thought to be a good option for orthopedic implants in the areas of bone remodeling and hard tissue regeneration. Additionally, they are frequently used in diverse medical applications, including drug delivery, biocompatible polymer-ceramic composites, and bioactive coating of metallic implants [7].

Because silicon ions play a significant role in metabolism during bone growth and cell proliferation, silicate ceramics have been discovered to generate apatite at a higher rate than hydroxyapatite (HAp) and other glass ceramics [8, 9]. Finally, calcium phosphates doped with silicon are showing better bioactivity than silicon-free calcium phosphates [3, 10].

Bioactive materials were identified among the silicate biomaterials, including AKT ($Ca_2MgSi_2O_7$), BR ($Ca_7MgSi_4O_{16}$), hatrurite (Ca_3SiO_5), monticellite ($CaMgSiO_4$), DPS ($CaMgSi_2O_6$), wollastonite ($CaSiO_3$),

* Corresponding author. *E-mail address:* Aidin.doroudi.i@gmail.com (A. Doroudi)
Received 2 January 2024; Received in revised form 29 February 2024; Accepted 3 March 2024.

https://doi.org/10.53063/synsint.2024.41210

larnite (Ca_2SiO_4), and hatrurite (Ca_3SiO_5). Due to their strong in-vitro bioactivity and biocompatibility [11, 12], silicate ceramic materials based on calcium and magnesium have received a lot of interest in the last decade when used as bulk materials or composites in simulated body fluid (SBF) [3].

Obtaining novel biomaterials for tissue engineering stands as one of the foremost challenges within the scientific community today. Because of their superior mechanical properties [13–15], appropriate degradability rate [16–18], high biocompatibility, bioactivity, and biodegradability [19–21], and frequent comparisons with calcium silicates ($CaSiO_3$) and CaPs ($Ca_3(PO_4)_2$) [22], bioceramics based on CMSs are thus being investigated more and more after their use in medicine.

The ceramic elements of the ternary system $CaO–SiO_2–MgO$, including DPS, AKT, and BR are also included in the family of calcium silicates [23–25]. Because of their multifunctional qualities, which include promoting the mineralization process through the deposition of apatite [26] and enhancing cell differentiation and proliferation [27], they are recommended as candidates for developing materials appropriate for treating bone tissue injuries and its regeneration [24, 25, 28]. It is reported that Mg-based Ca-silicates show promising outcomes in terms of cell adhesion, proliferation, and differentiation as well as mechanical strength, bioactivity, and antibacterial activity [29].

There are several ways to prepare these CMS, including the spray pyrolysis technique, the solid-state reaction [30, 31], the co-precipitation route [22], the sol-gel approach, and others [32, 33], but the most popular and straightforward method is the well-known wet-chemistry protocol, which entails changing from a sol to a gel and then finishing it with a heat treatment [34, 35].

In contrast, additive manufacturing technology (AMT) provides the opportunity to accurately duplicate a specific geometry directly from a bone defect through the incremental addition of material. AMT proves especially beneficial in the creation of intricate and hole-filled structures intended for bone restoration. Within the framework of ceramic ink-based material extrusion 3D printing, the binding agent, combined with ceramic ink, is extruded via a micro-nozzle to generate a filament that is then applied onto the substrate, thereby embedding the corresponding cross-sectional shape of a 3D model of the object under construction within the layer [36, 37].

Previous articles have shown that the synthesis method of CMS is of great importance to show suitable characteristics for specified applications such as bone tissue engineering and dental applications. In this review, we provide a thorough review of 3D-printed CMS ceramics from the perspective of BTE and dental implants.

2. Synthesis of CMS scaffolds

There are several traditional synthesis approaches for CMS scaffolds each offering unique advantages and challenges in tailoring the properties of the resulting scaffolds.

2.1. Space holder Method

There has been much written about the space holder method, which uses a volatile or solute material–like starch, carbamide, ammonium bicarbonate, or sodium chloride–as a space holder [38–40]. The method is as follows: space holder particles (of varying sizes and shapes) are combined with metal or ceramic powders, the powder mixture is compacted, and space holder materials are leached or evaporated to leave a high-volume proportion of porosity while the sintering process. Samples are given good mechanical properties and secondary porosity is reduced by sintering [38, 41, 42].

Generally speaking, spacers come in two varieties: soluble pore-forming particles like sodium chloride, which dissolve and are removed by a solvent, and volatile pore-forming particles like ammonium bicarbonate, which are burned out during sintering process or eliminated by raising the temperature before the sintering process. Sodium chloride is the material of choice for space holders among the others stated because it is readily available, inexpensive, rigid, and readily soluble in water. This method allows the spacer to directly influence most of the final scaffold properties, including pore shape, size, and porosity. Therefore, the selection of the appropriate spacer, its quantity, and the even powder mixing and spacer are the most substantial factors [41].

Utilizing an amalgamator, BR powders and NaCl are combined in a polyethylene container to create BR scaffolds utilizing the Space Holder Method. A final porosity of 80–90% is attained by adjusting the NaCl volume percentage. The density of each component determines the wt% of BR powder to space former. 2 wt% vegetable oil is added to the mixture to guarantee adequate adhesion and avoid agglomeration. After that, the powders are uniaxially compressed for a few minutes at pressures less than 50 MPa into cylindrical samples, followed by sintering these green samples. After that, the sintered samples are submerged in double deionized water, changing the water every 6 hours, to remove the NaCl space holder [41].

Spherical nanoparticle DPS powders with particle sizes smaller than 50 nm are used to create diopside scaffolds. Spacers with particle sizes ranging from 400 to 600 μm are used, such as NaCl and NH_4HCO_3. It is essential to use the right ratios of spacers to diopside powder to reach the desired porosity levels, which range from 60–90%. To lower the amount of pressure needed during the pressing stage, food-grade sunflower oil is added to the powders after they have been well mixed to create a homogenous mixture. Cold compaction is performed using a cylindrical die under specified pressures. Sintering processes vary depending on the type of spacer used. Removal of spacers is achieved by immersing sintered samples in deionized water or through heating. The final scaffolds are cooled to room temperature at a rate of 10 °C/min post-sintering. [40]

2.2. Electrospinning technique

Electrospinning is the most widely used technology for producing nanoparticles that are integrated into nanofibrous scaffolds due to its low setup costs and simplicity of use. Using an electrospinning method, Kouhi et al. created PHBV nanofibrous scaffolds containing treated BR nanoparticles. In their investigation, BR nanoparticles were combined with PHBV nanofibers after being altered using GPTMS [43, 44]. They found that the PHBV/G-BR scaffold indicated better mechanical qualities than PHBV and PHBV/BR, especially at higher nanoparticle concentrations.

To prepare nanocomposite fibrous PCL-DPS scaffolds, Hosseini et al. [45] prepared a 12 wt% PCL solution in a chloroform/methanol mixture (9:1 ratio), ensuring complete dissolution. They incorporated diopside nanopowder into the solution and sonicated it for 1 h for even dispersion. They employed a syringe pump to feed the polymer suspensions. Maintaining a voltage of about 20 kV with a needle-to-collector distance of about 15 cm, they set the flow rate at about

0.3 ml/h during electrospinning. Finally, they deposited the fibers onto Al-foil as a collector and dried the resulting scaffolds overnight under vacuum conditions to remove residual solvent.

Besides traditional methods, the additive manufacturing method has emerged as one of the most promising methods for synthesizing CMS materials for biomedical applications and implants.

2.3. 3D printing

To effectively stimulate bone ingrowth and bone support, bioceramic implants must have particular shapes and provide structural support to replace the deficiency area. 3D printing is a new and innovative manufacturing technique that has great potential in several fields, including bone tissue engineering and dentistry [46–48]. A range of customized porous ceramic scaffolds have been designed and produced for dental and bone regeneration applications using 3D printing technologies [49, 50]. According to recent investigations, bioceramic scaffolds with 3D porosity possess mechanical strength appropriate for use as dental and bone implant materials, and they can facilitate cell growth and tissue growth [51–55].

3. Properties of 3D-printed CMS compounds

3.1. 3D-printed CMS mechanical properties

It is reported that the mechanical property of CMS bioceramics is superior to phosphate bioceramics [3]. In comparison to $CaSiO_3$ and bioglass scaffolds, CMS scaffolds, particularly DPS scaffolds, have higher mechanical strength and mechanical stability. DPS scaffolds show promise as bioactive materials for bone tissue creation since they are more mechanically strong and have comparable cytocompatibility to HA scaffolds [56].

It is also reported that the higher temperature facilitates sintering and material diffusion, both of which improve a material's mechanical properties as it operates under continuous loads. [35] Liu et al. produced the triply periodic minimal surface (TPMS) model scaffolds with porosity of 50%, 60%, and 70% (Fig. 1) [54]. They compared the mechanical properties of samples with open-rod samples (Fig. 2).

3.2. Biocompatibility

Comparing CMS to calcium phosphates, the former has a slower degradation rate. Because of the silicon-rich layer that both stimulates and regulates the apatite precipitation formed on the surface upon the scaffold's immersion in SBF, the bio-ceramic surface exhibits improved in-vitro bioactivity. While phosphate bio-ceramic (bioresorbable) causes natural tissues to infiltrate and replace pores, silicate bioactive-ceramic exhibits superior interfacial bonding with natural tissue [57]. Comparing bioactive silicates including Ca, Mg, and Si to CaPs, which are clinically utilized in biomedical applications, the former show better mechanical properties like bending strength, Young's modulus, and fracture toughness [3, 58].

Because bioactive silicate ceramics are osteoconductive, bone can develop on its surface at the natural interface between implants and

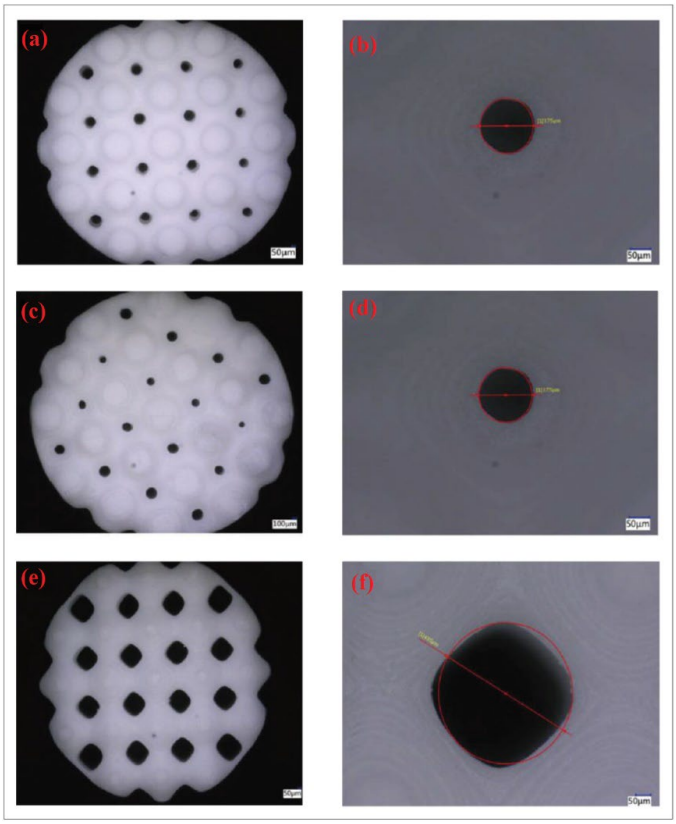

Fig. 1. The surface topography of a BR model holder fabricated using a 3D printing technique. The following are the porosities of the apertures: a, b) 175 μm, 50%; c, d) 310 μm, 60%; and e, f) 435 μm, 70% [54].

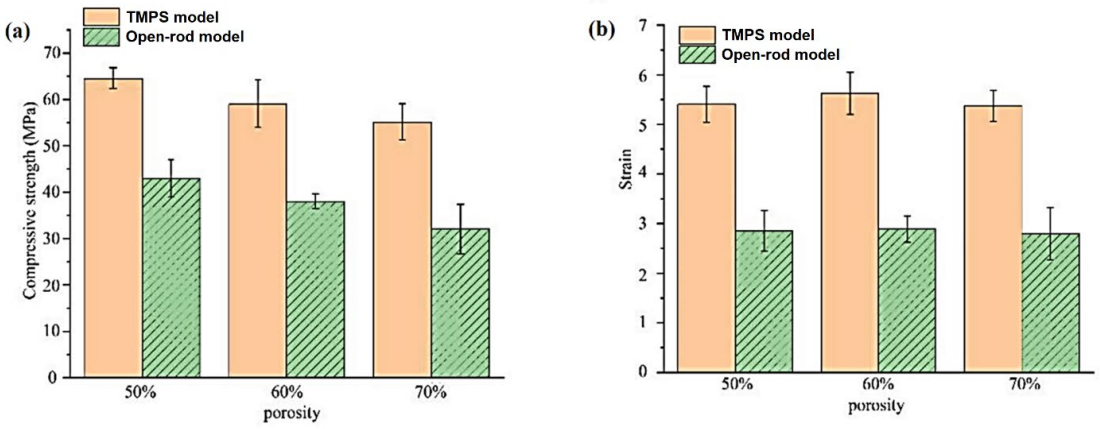

Fig. 2. The scaffolds' mechanical properties at different porosities: a) ultimate tensile strength and b) strain at support collapse (orange represents TPMS model support, green represents open-rod model support) [54].

bone. Osteoblast cell division, vascularization, extracellular matrix (ECM) proteins, and growth factor (insulin-like growth factor, or IGF) are all induced by the dissolution of Ca, Mg, and Si ions from CMS ceramics. It was discovered that the bioglass disintegration products upregulated genes and raised intracellular calcium [59–61].

Human osteoblast cells have been demonstrated to activate type I collagen protein in response to 10 mM silicic acid generated from silicates [62]. An optimal alternative material for bone grafts that serves as a template for bone growth must include an interconnected porous network structure to facilitate cell migration, vascularization, and, bone growth. Aside from sharing a mechanical load with the host bone, it must be biocompatible, bioactive, and attached to the host tissues. It needs to stimulate osteogenesis, break down gradually, and be remodeled by osteoclast activity [3, 63, 64].

AKT, one of the few binary and ternary silicates based on calcium and magnesium, demonstrates unique biological stimulation in enhancing osteogenic differentiation and cell proliferation because it releases the required ions into the body fluid at a certain concentration level from the ceramic [3, 65]. MC3T3-E1 cells' differentiation, and mineralization as well as ALP activity were all made possible by

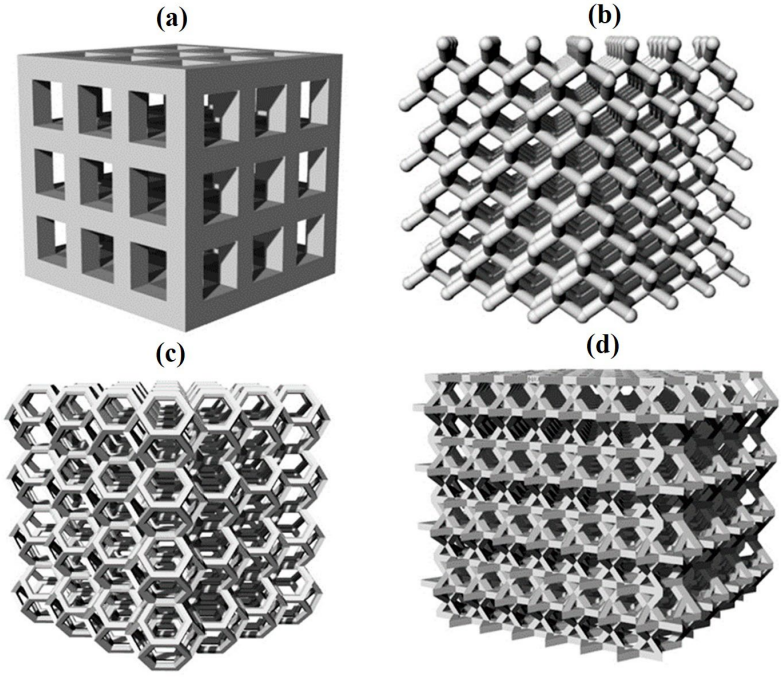

Fig. 3. Four types of lattice-based cellular assemblies were used for the scaffolds: a) cubic, b) diamond, c) Kelvin, and d) Kagome [78].

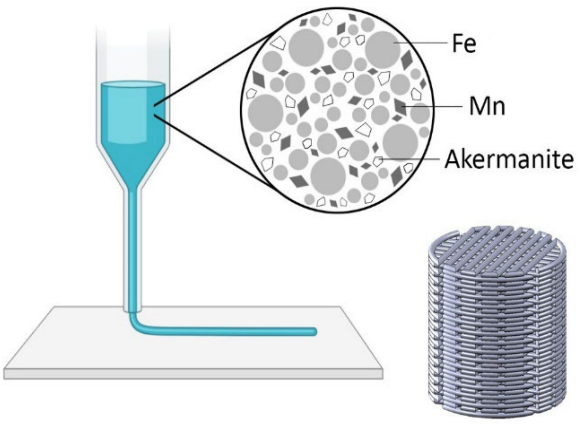

Fig. 4. Schematic of scaffold design and extrusion-based 3D printing [78].

diopside scaffolds. Additionally, it was engaged in the angiogenesis and adhesion of human adipose-derived stem cells (hAECs) and L-929 fibroblast cell lines, respectively. Also, it was sufficiently implanted with newly generated bone in-vivo in a monkey's mandible and a rabbit's jaw bone. AKT was found to promote the growth of hASCs, human bone marrow stromal cells (hBMSC), human periodontal ligament cells (hPDLCs), L-929 cell lines, and human aortic endothelial cells (hAECs). In New Zealand rabbits, it affects the osteogenesis and angiogenesis of hAECs and positively influences the development of hASCs via the extracellular signal-released kinase signaling pathway [3, 66].

4. Applications of 3D-printed CMS materials

Bone abnormalities resulting from diseases, trauma, aberrant skeletal development, and metabolic disorders have a substantial negative influence on the life quality of patients. The repair of these defects requires mechanical and structural support for the injured bone, preferably in the form of filler material. In addition to osteoinductive chemicals to encourage cell differentiation, this material should have an osteoconductive matrix to support bone cell growth and the creation of a three-dimensional bone structure. Autografts are frequently utilized, although they have disadvantages such as the potential for illness, difficulties with shape, and additional bone injury during transplantation. Bone tissue engineering attempts to overcome these shortcomings by functionally regenerating bone by modeling natural tissues. An essential component of this strategy, scaffolds imitate the extracellular matrix to provide structural support and improve the development of new bone. Scaffolds are generally made of natural polymers that are biocompatible and biodegradable, and they are strengthened with bioactive ceramics [67–70].

Bioceramic materials based on CaP, like HAp and β-tricalcium phosphate (β-TCP), exhibit potential for bone restoration as they resemble biological apatites [71–73]. Nevertheless, they have shortcomings such as low osteoinductivity, poor bone-bonding ability, delayed disintegration, and insufficient compressive strength [74]. Because of its higher rate of degradation, biodegradability without cytotoxicity, and tunable mechanical properties, AKT has emerged as a possible substitute [31]. Ca^{+2}, Si^{+4}, and Mg^{+2}ions make up AKT, which can be tailored to meet the needs of bone regeneration. One essential component of bioactivity for bone regeneration is the stimulation of cell and tissue contact by these ions. It has been discovered that AKT promotes the growth and differentiation of several cell types, including human aortic endothelial cells, bone marrow-derived stromal cells, and adipose-derived stem cells. Studies reveal that when it comes to bone production and healing, scaffolds based on AKT work better than those based on CaP [70, 75].

The creation of a porous scaffold utilizing complementary techniques like 3D printing and freeze-drying technologies is one way to restore the injured bone. These methods, which use bioactive ceramic and polymer, enhance the broken and fractured parts quickly for faster healing of bone lesions. In addition to the polymeric component, AKT bioceramic has been utilized as a bioactive calcium silicate bioceramic. The porous scaffolds were created by Dong et al. [76] employing solid work software that had a Gyroid form and a suitable porosity. The produced Gyroid scaffold was printed with Electroconductive Polylactic Acid (EC-PLA) in a 3D printer, and it was subsequently coated with a polymeric solution that included different concentrations of bioceramic AKT for reinforcement.

The porous-coated scaffold's mechanical properties demonstrated a stress endurance of up to 30 MPa. Maximum (max.) displacement was 0.006 mm, max. stress and strain were about 30 MPa, and 0.0008, respectively. The max. stress endurance of approximately 32 MPa with 46% porosity was found to be the mechanical properties of the porous scaffold containing 10 wt% AKT. Overall, they realized that the porous scaffold created by freeze-drying and 3D printing technology can be utilized to replace damaged bones with bioceramics made of 3D-printed EC-PLA covered with 10% AKT, which has enough mechanical and biological properties for orthopedic applications [76].

Ke et al. [77] used 3D printing and low-melting BG to create the AKT ceramic-based porous cages. The intervertebral disc trauma model was

Fig. 5. An extrusion-based 3D-printed hip stem and a similarly fabricated acetabular cup [78].

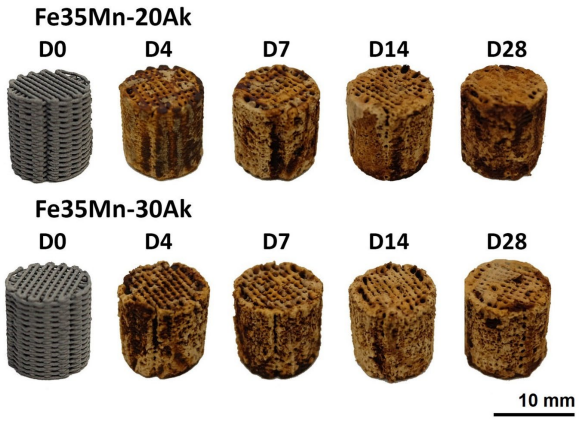

Fig. 6. The scaffolds' visual inspection at various times before and after in vitro biodegradation [78].

used to test the spinal fusion and assess the osteogenic cell adhesion on the cages in vitro. According to the findings, bioceramic cages with 15% or 30% BG added (aka AKT/BG15, AKT/BG30) had a compressive strength that was 2–5% higher than that of pure AKT cages (or AKT/BG0) [77]. Osteogenic cell growth and ALP expression were significantly enhanced by the surface of AKT/BG15 and AKT/BG30 cages compared to porous β-TCP cages. The AKT/BG15 and AKT/BG30 effectively promoted the new bone tissue formation and enhanced the recovery of spinal biomechanics, according to histological and biomechanical research. 4–6 of the rabbits, in the AKT/BG15 and AKT/BG30 cage groups, showed signs of a successful fusion. On the other hand, at 12 weeks after surgery, only 0–1 of the original seeded TCP and AKE/BG0 cages showed fusion. To summarize, the cages made of AKT showed a greater ability to regenerate bone in an intervertebral disc trauma model. This suggests that the cages could be a viable option for enhancing spinal fusion surgery [77].

This study demonstrates how to manufacture 3D scaffolds with hierarchically porous structures using AKT, a bioceramic that has great promise for stereolithography. By using 3D models that corresponded to several lattice configurations (cubic, diamond, Kelvin, and Kagome), the macroporosity was designed (Fig. 3) [78].

To achieve micro-scale porosity, green scaffolds Dasan et al. [20] created using flame-synthesized glass microbeads containing 10% silicone resin, which were subsequently fired at 1100 °C in the air to transform them into the desired bioceramic phase. After heat treatment, no chemical reaction was seen between the glass microspheres that crystallized into AKT and the silica that resulted from silicone oxidation. By acting as a binder between neighboring microspheres, silica improved the formation of microporosity. Rhodamine B solution infiltration verified the creation of "spongy" struts. With a porosity of 68–84%, the sintered porous scaffolds had a compressive strength of up to 0.7 MPa. To address the unmet clinical needs associated with Fe-based biomaterials for bone regeneration, such as low biodegradation rate, MRI incompatibility, mechanical properties, and limited bioactivity, Putra et al. [78] made porous FeMn-AKT composite scaffolds by extrusion-based 3D printing (Fig. 4).

Putra et al. [78] created porous FeMn-AKT composite scaffolds using extrusion-based 3D printing to address the unmet clinical demands related to Fe-based biomaterials for bone regeneration, such as MRI incompatibility, low biodegradation rate, restricted bioactivity, and mechanical characteristics (Fig. 4). Inks with combinations of Fe, 35 wt% Mn and 20 or 30 vol% AKT powder were created. Apart from the cylindrical samples, the extrusion-based 3D printing technique showed the ability to create geometrically complex implants, such as the hip stem and acetabular components (Fig. 5) [78].

To produce scaffolds with interconnected porosity of about 70%, 3D printing was optimized in conjunction with the debinding and sintering processes. Nesosilicate phases and the γ-FeMn phase were both present in the Fe-matrix of the composites. The former rendered the composites paramagnetic, making them suitable for MRI. The composites containing 20 and 30 vol% AKT had in vitro biodegradation rates of about 0.25 and 0.27 mm/y, respectively. These rates are within the optimal range for bone replacement [78]. Despite 28 days of in vitro biodegradation, the yield strengths of the synthesized porous composites remained within the range of the values of the trabecular bone (Fig. 6). The obtained results showed that all of the composite scaffolds promoted the proliferation, adhesion, and osteogenic differentiation of preosteoblasts. Additionally, osteopontin was found in the cells' extracellular matrix on the scaffolds [78].

The 3D printing technique creates 3D objects, that can be utilized as orthopedic implants and plates by depositing polymeric biomaterials layer by layer (Fig. 7); however, the implants or plates that are 3D-printed might not have the qualities needed to bind with host tissue. One suitable technique to modify plates to get around this problem is to coat them with nanofibers [79].

Fig. 7. The 3D-printed orthopedic plate [79].

In the study performed by Zhang et al. [79] an orthopedic plate was coated with PCL/AKT nanofibers after being 3D-printed using PLA. 8 wt% PCL and 3 wt% nAKT were present in the mixture, and the PCL/AKT nano-fibers diameter was roughly 250 nm ± 30 nm. The y increased the max. pressure force by 16.83% when PCL was added to PLA. The PLA + PCL sample's max. pressure force was further increased by 4.7% by the addition of nAKT. Additionally, the max. bending flexural force was increased by 21.06% when PCL was added to PLA. Additionally, the highest bending flexural force was increased by 21.39% by the addition of nAKT to the PLA + PCL sample [79].

Table 1 summarizes the recent studies performed to produce CMS scaffolds via the 3D printing method. These studies highlight various parameters such as base material, mechanical properties, and biocompatibility assessments. The studies demonstrate the versatility of 3D printing in fabricating CMS scaffolds with controlled architecture and functionality, paving the way for advanced tissue regeneration strategies.

Table 1. Most recent studies about the production of CMS scaffolds via the 3D printing method.

CMS	No.	Material*	Potential application	Main results	Ref.
AKT	1	45S5 bioglass/ AKT	Repairing the load-bearing segmental bone defects	45S5 BG containing 4 wt% B_2O_3 analogs could easily reinforce AKT ceramics at a content of 20–40 wt%. High-strength porous scaffolds with compressive strength (roughly 36 MPa) 10 times higher than those of pure AKT porous ceramics could be created using extrusion-based 3D printing and pressureless sintering. The porous ceramic composites demonstrated a slower rate of biodegradation in vitro (in Tris buffer), but this had no effect on the porous formulation's strength over an extended period (6 weeks). It is suggested that creating high-strength bioceramic scaffolds via 3D printing and NCS-assisted sintering is a viable substitute that may be used to fix load-bearing segmental bone lesions.	[36]
	2	CS/AKT-TiO_2	Bone tissue engineering load-bearing applications	The created 3D-composite scaffolds' mechanical, biological, and morphological characteristics closely resembled those of real bone tissue.	[70]
	3	BG-AKT	Spinal fusion	Bioceramic cages with 15% or 30% BG could have a compressive strength that is two or five times higher than that of pure AKT cages.	[77]
	4	FeMn-AKT	Bone substitute	The composites containing 20 and 30 vol% AKT had in vitro biodegradation rates of 0.24 and 0.27 mm/y, respectively. These rates were within the optimal range for bone replacement.	[78]
	5	PCL/AKT coated PLA	Orthopedic plate	The max. pressure force is increased by 16.83% when PCL is added to PLA. Additionally, the PLA + PCL sample's max. pressure force is increased by 4.72% by adding nAKT. Additionally, the max. bending flexural force is increased by 21.06% when PCL is added to PLA. Additionally, the max. bending flexural force is increased by 21.39% by the addition of nAKT to the PLA + PCL sample.	[79]
	6	Black AKT	Regenerative medicine	Scaffolds because of surface defects that activate the bone morphogenetic protein 2 signaling pathway and encourage osteogenic differentiation of mesenchymal stem cells in rabbit bone, hence accelerating the production of new bone in vivo.	[80]
	7	BCN-AKT	Cancer treatment and bone regeneration	Notably, BCN nanosheets' potent light absorption ability allowed for the special photothermal efficiency of BCN@AKT scaffolds for osteosarcoma therapy.	[81]
	8	β-TCP/15% AKT	Bone repair	The composite scaffold's grain size increased and its micropore count decreased upon the addition of AKT. The addition of AKT significantly enhanced the composite scaffold's mechanical properties, leading to a 20% gain in strength.	[82]
	9	Iron/AKT	Bone regeneration	Up to 2.6 times faster than the biodegradation rate of geometrically equivalent pure Fe, the composites' in vitro biodegradation rates showed improvement. Even after 28 days of biodegradation, the scaffolds' elastic moduli and yield strengths were still within the range of the mechanical properties of the cancellous bone. Higher levels of cell proliferation and enhanced MC3T3-E1 cell adherence were shown by the composite scaffolds (10–20 vol% AKT). The activity of Collagen type-1 cellular secretion and alkaline phosphatase on the composite scaffolds (10–20 vol% AKT) were comparable to Ti6Al4V in osteogenic media and higher, respectively.	[83]
	10	AKT	Bone tissue engineering	The porous bioactive ceramic scaffolds show promise for promoting cell adhesion and proliferation, mineralization capacity, and bacteriostatic qualities. They also have sufficient compressive strength (up to 3.5 MPa).	[84]
BR	11	$MoSe_2$ functionalized BR	Bone tumor therapy	The MS-BR scaffolds can efficiently kill HeLa and MG-63 cells while encouraging osteoblast adhesion and growth. BR and MS-BR both have advantageous osteogenic properties.	[52]
	12	BR-O	Bone tissue engineering	By improving the polarization of M2 macrophages, BR-O scaffolds contribute to the promotion of critical-sized bone defects in vivo through immunomodulatory effects.	[55]
	13	Sr-doped BR-PCL-PLA	Bone regeneration	The PLA/PCL/BR-5%Sr nanocomposite scaffolds showed an increase in both mechanical strength and degradation rate. Human osteoblast viability and proliferation were supported by the scaffolds. The scaffolds with the greatest potential for bone tissue regeneration were those that contained BR-Sr ceramic nanoparticles.	[85]
	14	BR	Cartilage and subchondral bone regeneration	A clever approach to treating osteochondral lesions is the use of 3D-printed scaffolds with micro/nanostructured surfaces, which can physiologically meet the needs for concurrent repair of both cartilage and subchondral bone.	[86]
	15	Fe_3O_4-BR	Hyperthermia applications	The effect of MNP wt. fraction on the nonlinear frequency of the bionanocomposite implant becomes more significant with increasing max. deflection.	[87]

Table 1. Continued.

CMS	No.	Material*	Potential application	Main results	Ref.
DPS	16	DPS	Bone tissue engineering	There was a progressive improvement in both compressive strength and fracture toughness, rising from 5.96 ± 0.88 MPa to 10.87 ± 0.55 MPa, by increasing energy density.	[14]
	17	HA-DPS	-	MS doping plays an important role in the reduction of grain size from 12 µm to 6 µm. The composite scaffold exhibits a 59.15% increase in compressive stress compared to the pure HA scaffold. To achieve biocompatibility, DPS can be added to HA during the doping phase at a weight percentage of 30%.	[88]
	18	Wollastonite-DPS	Bone tissue engineering	All the samples showed high strength-to-density ratios. The firing temperature was conditioned by the varying requirements of several 3D printing technologies concerning particle size and the sensitivity of the employed glasses to surface nucleation: samples made by DLP, which used finer powders more prone to crystallization, could be burned at higher temperatures; samples made by 3D printing, which used coarser particles resulting in restricted crystallization, were better suited for low-temperature firing (between 800–900 °C).	[89]
	19	Wollastonite-DPS	Treatment of osteonecrosis of the femoral head work as a bioceramic rod.	With an increase in CSM10 content from 0% to 30%, the secondary phase (i.e., 10% Mg substituting calcium silicate; CSM10) could easily improve the sintering property of the bioceramic composites (DIO/CSM10-x, x = 0–30). Additionally, the presence of CSM10 increased the ability of biomimetic apatite mineralization in the scaffolds' pore struts. The 3D-printed porous bioceramics' flexible strength (between 12.5–30 MPa) and compressive strength (between 14–37 MPa) significantly increased as the CSM10 content increased. Additionally, the compressive strength of DIO/CSM10-30 indicated a limited decay (from 37 to 29 MPa) in the Tris buffer solution over an extended period (8 weeks).	[90]

* AKT: Akermanite, BCN: Borocarbonitrides, CS: Chitosan, TCP: Tri-calcium phosphate, BG: Bioactive glass, PCL: polycaprolactone, PLA: Polylactic acid, BR: Bredigite, BR-O: Structurally ordered bredigite, DPS: Diopside.

5. Conclusions and future insights

In conclusion, this mini-review highlights the promising advancements in the 3D printing of CMS materials and underscores their significant potential across various domains. Moving forward, it is essential to address key challenges, such as achieving optimal mechanical properties, enhancing biocompatibility, and scaling up production processes for practical applications.

Furthermore, novel CMS compositions, improved printing methods that allow fine-grained control over scaffold construction, and multi-functional CMS-based composites for improved performance could be the main areas of future research. Researcher, industry, and regulatory collaboration are essential to fostering innovation, standardizing fabrication processes, and easing the transition of 3D-printed CMS materials from lab settings to practical uses. In the end, further developments in this emerging subject have the potential to transform a variety of industries and solve urgent societal issues.

CRediT authorship contribution statement

Aidin Doroudi: Supervision, Writing – original draft.
Preeti Lata Mahapatra: Visualization; Writing – review & editing.
Fatemeh Bakhshi: Project administration, Writing – original draft.

Data availability

Data sharing is not applicable – no new data is generated.

Declaration of competing interest

The authors declare no competing interests.

Funding and acknowledgment

The authors received no financial support for the research, authorship, and/or publication of this article.

References

[1] L.L. Hench, R.J. Splinter, W.C. Allen, T.K. Greenlee, Bonding mechanisms at the interface of ceramic prosthetic materials, J. Biomed. Mater. Res. 5 (1971) 117–141. https://doi.org/10.1002/jbm.820050611.
[2] C. Wu, J. Chang, Degradation, bioactivity, and cytocompatibility of diopside, akermanite, and bredigite ceramics, J. Biomed. Mater. Res. B. 83B (2007) 153–160. https://doi.org/10.1002/jbm.b.30779.
[3] S.K. Venkatraman, S. Swamiappan, Review on calcium-and magnesium-based silicates for bone tissue engineering applications, J. Biomed. Mater. Res. A. 108 (2020) 1546–1562. https://doi.org/10.1002/jbm.a.36925.
[4] M. Vallet-Regí, Ceramics for medical applications, J. Chem. Soc. Dalton Trans. (2001) 97–108. https://doi.org/10.1039/B007852M.
[5] S. Amirfarhangi, A. Vakili, L. Radfar, N. Tajbakhsh, Golden proportion and facial esthetic, the harmony and surgical considerations: A review, World J. Biol. Pharm. Health Sci. 11 (2022) 018–021. https://doi.org/10.30574/wjbphs.2022.11.1.0097.
[6] A. Shahbaz, N. Tajbakhsh, A. Doroudi, F. Bakhshi, S. Ranjbar, Bredigite-containing materials for regenerative medicine applications: A rapid review, J. Compos. Compd. 5 (2023) 190–199. https://doi.org/10.61186/jcc.5.3.4.

[7] F. Tavangarian, R. Emadi, Improving degradation rate and apatite formation ability of nanostructure forsterite, Ceram. Int. 37 (2011) 2275–2280. https://doi.org/10.1016/j.ceramint.2011.03.022.
[8] S. Ni, J. Chang, In vitro Degradation, Bioactivity, and Cytocompatibility of Calcium Silicate, Dimagnesium Silicate, and Tricalcium Phosphate Bioceramics, J. Biomater. Appl. 24 (2009) 139–158. https://doi.org/10.1177/0885328208094745.
[9] A.H. Shahbaz, M. Esmaeilian, R. NasrAzadani, K. Gavanji, Effect of MgF2 addition on the mechanical properties of hydroxyapatite synthesized via powder metallurgy, J. Compos. Compd. 1 (2019) 16–21. https://doi.org/10.29252/jcc.1.1.3.
[10] H. Ghomi, M. Jaberzadeh, M.H. Fathi, Novel fabrication of forsterite scaffold with improved mechanical properties, J. Alloys Compd. 509 (2011) L63–L68. https://doi.org/10.1016/j.jallcom.2010.10.106.
[11] R. Choudhary, L. Ravi, S. Swamiappan, Silicate ceramics and its composites for hard tissue applications, Eco-Friendly Nano-Hybrid Materials for Advanced Engineering Applications, Apple Academic Press. (2017) 131–182. https://doi.org/10.1201/9781315366531-8.
[12] M. Diba, M. Kharaziha, M.H. Fathi, M. Gholipourmalekabadi, A. Samadikuchaksaraei, Preparation and characterization of polycaprolactone/forsterite nanocomposite porous scaffolds designed for bone tissue regeneration, Compos. Sci. Technol. 72 (2012) 716–723. https://doi.org/10.1016/j.compscitech.2012.01.023.
[13] Z. Han, C. Gao, P. Feng, Y. Shen, C. Shuai, S. Peng, Silicon carbide whiskers reinforced akermanite scaffolds for tissue engineering, RSC Adv. 4 (2014) 36868–36874. https://doi.org/10.1039/C4RA07474B.
[14] L. Tingting, D. Youwen, G. Chengde, F. Pei, C. Shuai, P. Shuping, Analysis of 3D printed diopside scaffolds properties for tissue engineering, Mater. Sci. 21 (2015) 590–594. https://doi.org/10.5755/j01.ms.21.4.9845.
[15] A. Dasan, H. Elsayed, J. Kraxner, D. Galusek, E. Bernardo, Hierarchically porous 3D-printed akermanite scaffolds from silicones and engineered fillers, J. Eur. Ceram. Soc. 39 (2019) 4445–4449. https://doi.org/10.1016/j.jeurceramsoc.2019.06.021.
[16] Z. Han, P. Feng, C. Gao, Y. Shen, C. Shuai, S. Peng, Microstructure, mechanical properties and in vitro bioactivity of akermanite scaffolds fabricated by laser sintering, Bio-Med. Mater. Eng. 24 (2014) 2073–2080. https://doi.org/10.3233/BME-141017.
[17] M.R. Shahrouzifar, E. Salahinejad, Strontium doping into diopside tissue engineering scaffolds, Ceram. Int. 45 (2019) 10176–10181. https://doi.org/10.1016/j.ceramint.2019.02.067.
[18] S. Pang, D. Wu, F. Kamutzki, J. Kurreck, A. Gurlo, D.A.H. Hanaor, High performing additively manufactured bone scaffolds based on copper substituted diopside, Mater. Des. 215 (2022) 110480. https://doi.org/10.1016/j.matdes.2022.110480.
[19] Z. Ba, Z. Chen, Y. Huang, D. Feng, Q. Zhao, et al., Nanoporous diopside modulates biocompatibility, degradability and osteogenesis of bioactive scaffolds of gliadin-based composites for new bone formation, Int. J. Nanomed. (2018) 3883–3896. https://doi.org/10.2147/IJN.S162262.
[20] A. Dasan, J. Kraxner, L. Grigolato, G. Savio, H. Elsayed, et al., 3D Printing of Hierarchically Porous Lattice Structures Based on Åkermanite Glass Microspheres and Reactive Silicone Binder, J. Funct. Biomater. 13 (2022) 8. https://doi.org/10.3390/jfb13010008.
[21] M. Hafezi-Ardakani, F. Moztarzadeh, M. Rabiee, A.R. Talebi, M. Abasi-shahni, et al., Sol-gel synthesis and apatite-formation ability of nanostructure merwinite (Ca3MgSi2O8) as a novel bioceramic, J. Ceram. Process. Res. 11 (2010) 765–768
[22] M.S. Collin, S.K. Venkatraman, M. Sriramulu, S. Shanmugam, E.A. Drweesh, et al., Solution combustion synthesis of functional diopside, akermanite, and merwinite bioceramics: Excellent biomineralization, mechanical strength, and antibacterial ability, Mater. Today Commun. 27 (2021) 102365. https://doi.org/10.1016/j.mtcomm.2021.102365.
[23] M. Ansari, F. Malmir, A. Salati, Preparation and Characterization of Akermanite/Merwinite Scaffolds for Bone Tissue Repair, J. Biomim. Biomater. Biomed. Eng. 44 (2020) 73–81. https://doi.org/10.4028/www.scientific.net/JBBBE.44.73.
[24] M. Razavi, M. Fathi, O. Savabi, D. Vashaee, L. Tayebi, In vivo biocompatibility of Mg implants surface modified by nanostructured merwinite/PEO, J. Mater. Sci. Mater. Med. 26 (2015) 184. https://doi.org/10.1007/s10856-015-5514-3.
[25] Y. Hosseini, R. Emadi, M. Kharaziha, Surface modification of PCL-diopside fibrous membrane via gelatin immobilization for bone tissue engineering, Mater. Chem. Phys. 194 (2017) 356–366. https://doi.org/10.1016/j.matchemphys.2017.03.051.
[26] J. Ou, G.F. Yin, D.L. Zhou, X.C. Chen, Y.D. Yao, et al., Preparation of Merwinite with Apatite-Forming Ability by Sol-Gel Process, Key Eng. Mater. 330–332 (2007) 67–70. https://doi.org/10.4028/www.scientific.net/KEM.330-332.67.
[27] C. Shuai, Z. Han, P. Feng, C. Gao, T. Xiao, S. Peng, Akermanite scaffolds reinforced with boron nitride nanosheets in bone tissue engineering, J. Mater. Sci: Mater. Med. 26 (2015) 188. https://doi.org/10.1007/s10856-015-5513-4.
[28] G. Birhanu, M. Doosti-Telgerd, A. Zandi-Karimi, Z. Karimi, M. Porgham Daryasari, et al., Enhanced proliferation and osteogenic differentiation of mesenchymal stem cells by diopside coated Poly-L-lactic Acid-Based nanofibrous scaffolds, Int. J. Polym. Mater. Polym. Biomater. 71 (2022) 707–716. https://doi.org/10.1080/00914037.2021.1879078.
[29] S.K. Venkatraman, R. Choudhary, G. Krishnamurithy, H.R. Balaji Raghavendran, M.R. Murali, et al., Comparative investigation on antibacterial, biological and mechanical behaviour of monticellite and diopside derived from biowaste for bone regeneration, Mater. Chem. Phys. 286 (2022) 126157. https://doi.org/10.1016/j.matchemphys.2022.126157.
[30] H. Mohammadi, Y.M.B. Ismail, K.A. Shariff, A.F.M. Noor, Effect of substitutional Strontium on Mechanical Properties of Akermanite Ceramic Prepared by Solid-State Sintering, Mater. Today: Proc. 17 (2019) 929–936. https://doi.org/10.1016/j.matpr.2019.06.393.
[31] A.K. Sharafabadi, M. Abdellahi, A. Kazemi, A. Khandan, N. Ozada, A novel and economical route for synthesizing akermanite (Ca2MgSi2O7) nano-bioceramic, Mater. Sci. Eng: C. 71 (2017) 1072–1078. https://doi.org/10.1016/j.msec.2016.11.021.
[32] R. Choudhary, S. Koppala, S. Swamiappan, Bioactivity studies of calcium magnesium silicate prepared from eggshell waste by sol–gel combustion synthesis, J. Asian Ceram. Soc. 3 (2015) 173–177. https://doi.org/10.1016/j.jascer.2015.01.002.
[33] S. Yamamoto, N. Kawamura, T. Nonami, Diopside Synthesized by Sol-gel Method as Phosphorus Adsorption Material: Evaluation of Apatite Deposition in Pseudo Body Solution, Trans. Mater. Res. Soc. Jpn. 44 (2019) 17–23. https://doi.org/10.14723/tmrsj.44.17.
[34] R. Negrea, C. Busuioc, I. Constantinoiu, D. Miu, C. Enache, et al., Akermanite-based coatings grown by pulsed laser deposition for metallic implants employed in orthopaedics, Surf. Coat. Technol. 357 (2019) 1015–1026. https://doi.org/10.1016/j.surfcoat.2018.11.008.
[35] A.-E. Alecu, C.-C. Costea, V.-A. Surdu, G. Voicu, S.-I. Jinga, C. Busuioc, Processing of Calcium Magnesium Silicates by the Sol–Gel Route, Gels. 8 (2022) 574. https://doi.org/10.3390/gels8090574.
[36] X. Wang, L. Zhang, X. Ke, J. Wang, G. Yang, et al., 45S5 Bioglass analogue reinforced akermanite ceramic favorable for additive manufacturing mechanically strong scaffolds, RSC Adv. 5 (2015) 102727–102735. https://doi.org/10.1039/c5ra19272b.
[37] P.L. Mahapatra, R. Tromer, A. Jayakumar, G. Costin, B. Lahiri, et al., 3D-printed flexible energy harvesting devices designed using non-layered two-dimensional natural tourmaline silicates, J. Mater. Chem. C. 12 (2024) 3418–3429. https://doi.org/10.1039/D3TC04167K.
[38] Q. Fu, E. Saiz, M.N. Rahaman, A.P. Tomsia, Bioactive glass scaffolds for bone tissue engineering: state of the art and future perspectives, Mater. Sci. Eng: C. 31 (2011) 1245–1256. https://doi.org/10.1016/j.msec.2011.04.022.

[39] M. Abdellahi, A. Najafinezhad, H. Ghayour, S. Saber-Samandari, A. Khandan, Preparing diopside nanoparticle scaffolds via space holder method: Simulation of the compressive strength and porosity, J. Mech. Behav. Biomed. Mater. 72 (2017) 171–181. https://doi.org/10.1016/j.jmbbm.2017.05.004.
[40] H. Ghomi, R. Emadi, S.H. Javanmard, Fabrication and characterization of nanostructure diopside scaffolds using the space holder method: Effect of different space holders and compaction pressures, Mater. Des. 91 (2016) 193–200. https://doi.org/10.1016/j.matdes.2015.11.078.
[41] H. Ghomi, R. Emadi, Fabrication of bioactive porous bredigite (Ca7MgSi4O16) scaffold via space holder method, International J. Mater. Res. 109 (2018) 257–264. https://doi.org/10.3139/146.111597.
[42] A. Mansourighasri, N. Muhamad, A.B. Sulong, Processing titanium foams using tapioca starch as a space holder, J. Mater. Proc. Technol. 212 (2012) 83–89. https://doi.org/10.1016/j.jmatprotec.2011.08.008.
[43] M. Kouhi, M. Fathi, V. Jayarama Reddy, S. Ramakrishna, Bredigite Reinforced Electrospun Nanofibers for Bone Tissue Engineering, Mater. Today: Proc. 7 (2019) 449–454. https://doi.org/10.1016/j.matpr.2018.11.108.
[44] M. Kouhi, M. Fathi, M.P. Prabhakaran, M. Shamanian, S. Ramakrishna, Poly L lysine-modified PHBV based nanofibrous scaffolds for bone cell mineralization and osteogenic differentiation, Appl. Surf. Sci. 457 (2018) 616–625. https://doi.org/10.1016/j.apsusc.2018.06.239.
[45] Y. Hosseini, R. Emadi, M. Kharaziha, A. Doostmohammadi, Reinforcement of electrospun poly(ε-caprolactone) scaffold using diopside nanopowder to promote biological and physical properties, J. Appl. Polym. Sci. 134 (2017). https://doi.org/10.1002/app.44433.
[46] A. Khademhosseini, R. Langer, A decade of progress in tissue engineering, Nat. Protoc. 11 (2016) 1775–1781. https://doi.org/10.1038/nprot.2016.123.
[47] B. Baumann, T. Jungst, S. Stichler, S. Feineis, O. Wiltschka, et al., Control of Nanoparticle Release Kinetics from 3D Printed Hydrogel Scaffolds, Angew. Chem. Int. Ed. 56 (2017) 4623–4628. https://doi.org/10.1002/anie.201700153.
[48] N. Tajbakhsh, F. Delpisheh, N. Ghadimi, S. Ansari, Smile management: White esthetic, pink esthetic and facial attractiveness, a review of literature, Open Access Res. J. Biol. Pharm. 05 (2022) 046–050. https://doi.org/10.53022/oarjbp.2022.5.2.0054.
[49] Y. Zhang, D. Zhai, M. Xu, Q. Yao, H. Zhu, et al., 3D-printed bioceramic scaffolds with antibacterial and osteogenic activity, Biofabrication. 9 (2017) 025037. https://doi.org/10.1088/1758-5090/aa6ed6.
[50] I. Sabree, J.E. Gough, B. Derby, Mechanical properties of porous ceramic scaffolds: Influence of internal dimensions, Ceram. Int. 41 (2015) 8425–8432. https://doi.org/10.1016/j.ceramint.2015.03.044.
[51] R. Wang, P. Zhu, W. Yang, S. Gao, B. Li, Q. Li, Direct-writing of 3D periodic TiO2 bio-ceramic scaffolds with a sol-gel ink for in vitro cell growth, Mater. Des. 144 (2018) 304–309. https://doi.org/10.1016/j.matdes.2018.02.040.
[52] X. Zhang, Y. Li, X. Dong, H. Wang, B. Chen, et al., 3D-printed bioactive ceramic scaffolds with MoSe2 nanocrystals as photothermal agents for bone tumor therapy, RSC Adv. 12 (2022) 30588–30597. https://doi.org/10.1039/D2RA02942A.
[53] C. Qin, D. Che, D. Liu, Z. Zhang, Y. Feng, Preparation and characterization of different micro/nano structures on the surface of bredigite scaffolds, Sci. Rep. 13 (2023) 9072. https://doi.org/10.1038/s41598-023-36382-z.
[54] D. Liu, X. Zhou, F. Wang, Y. Feng, Y. Shi, Research and analysis of the properties of bredigite-based 3D-printed bone scaffolds, IJB. 9 (2023) 708. https://doi.org/10.18063/ijb.708.
[55] Y. Xuan, L. Li, C. Zhang, M. Zhang, J. Cao, Z. Zhang, The 3D-Printed Ordered Bredigite Scaffold Promotes Pro-Healing of Critical-Sized Bone Defects by Regulating Macrophage Polarization, Int. J. Nanomed. 18 (2023) 917–932. https://doi.org/10.2147/IJN.S393080.
[56] C. Wu, Y. Ramaswamy, H. Zreiqat, Porous diopside (CaMgSi2O6) scaffold: A promising bioactive material for bone tissue engineering, Acta Biomater. 6 (2010) 2237–2245. https://doi.org/10.1016/j.actbio.2009.12.022.
[57] J. Wei, F. Chen, J.-W. Shin, H. Hong, C. Dai, et al., Preparation and characterization of bioactive mesoporous wollastonite – Polycaprolactone composite scaffold, Biomaterials. 30 (2009) 1080–1088. https://doi.org/10.1016/j.biomaterials.2008.10.046.
[58] R. Emadi, S.I. Roohani Esfahani, F. Tavangarian, A novel, low temperature method for the preparation of ß-TCP/HAP biphasic nanostructured ceramic scaffold from natural cancellous bone, Mater. Lett. 64 (2010) 993–996. https://doi.org/10.1016/j.matlet.2010.01.085.
[59] L.L. Hench, I. Thompson, Twenty-first century challenges for biomaterials, J. Royal Soc. Interface. 7 (2010) S379–S391. https://doi.org/10.1098/rsif.2010.0151.focus.
[60] I.D. Xynos, A.J. Edgar, L.D.K. Buttery, L.L. Hench, J.M. Polak, Gene-expression profiling of human osteoblasts following treatment with the ionic products of Bioglass® 45S5 dissolution, J. Biomed. Mater. Res. 55 (2001) 151–157. https://doi.org/10.1002/1097-4636(200105)55:2<151::AID-JBM1001>3.0.CO;2-D.
[61] I.D. Xynos, A.J. Edgar, L.D.K. Buttery, L.L. Hench, J.M. Polak, Ionic Products of Bioactive Glass Dissolution Increase Proliferation of Human Osteoblasts and Induce Insulin-like Growth Factor II mRNA Expression and Protein Synthesis, Biochem. Biophys. Res. Commun. 276 (2000) 461–465. https://doi.org/10.1006/bbrc.2000.3503.
[62] I.D. Xynos, M.V.J. Hukkanen, J.J. Batten, L.D. Buttery, L.L. Hench, J.M. Polak, Bioglass ®45S5 Stimulates Osteoblast Turnover and Enhances Bone Formation In Vitro: Implications and Applications for Bone Tissue Engineering, Calcif. Tissue Int. 67 (2000) 321–329. https://doi.org/10.1007/s002230001134.
[63] J.R. Jones, Review of bioactive glass: From Hench to hybrids, Acta Biomater. 9 (2013) 4457–4486. https://doi.org/10.1016/j.actbio.2012.08.023.
[64] E. Fiume, J. Barberi, E. Verné, F. Baino, Bioactive Glasses: From Parent 45S5 Composition to Scaffold-Assisted Tissue-Healing Therapies, J. Funct. Biomater. 9 (2018). https://doi.org/10.3390/jfb9010024.
[65] H. Gu, F. Guo, X. Zhou, L. Gong, Y. Zhang, et al., The stimulation of osteogenic differentiation of human adipose-derived stem cells by ionic products from akermanite dissolution via activation of the ERK pathway, Biomaterials. 32 (2011) 7023–7033. https://doi.org/10.1016/j.biomaterials.2011.06.003.
[66] M. Diba, O.-M. Goudouri, F. Tapia, A.R. Boccaccini, Magnesium-containing bioactive polycrystalline silicate-based ceramics and glass-ceramics for biomedical applications, Curr. Opin. Solid State Mater. Sci. 18 (2014) 147–167. https://doi.org/10.1016/j.cossms.2014.02.004.
[67] A. Liu, M. Sun, X. Yang, C. Ma, Y. Liu, et al., Three-dimensional printing akermanite porous scaffolds for load-bearing bone defect repair: An investigation of osteogenic capability and mechanical evolution, J. Biomater. Appl. 31 (2016) 650–660. https://doi.org/10.1177/0885328216664839.
[68] L.D. Shea, D. Wang, R.T. Franceschi, D.J. Mooney, Engineered Bone Development from a Pre-Osteoblast Cell Line on Three-Dimensional Scaffolds, Tissue Eng. 6 (2000) 605–617. https://doi.org/10.1089/10763270050199550.
[69] K.J.L. Burg, S. Porter, J.F. Kellam, Biomaterial developments for bone tissue engineering, Biomaterials. 21 (2000) 2347–2359. https://doi.org/10.1016/S0142-9612(00)00102-2.
[70] B. Bulut, Ş. Duman, Evaluation of mechanical behavior, bioactivity, and cytotoxicity of chitosan/akermanite-TiO2 3D-printed scaffolds for bone tissue applications, Ceram. Int. 48 (2022) 21378–21388. https://doi.org/10.1016/j.ceramint.2022.04.104.
[71] P. Miranda, A. Pajares, E. Saiz, A.P. Tomsia, F. Guiberteau, Mechanical properties of calcium phosphate scaffolds fabricated by

robocasting, J. Biomed. Mater. Res. A. 85A (2008) 218–227. https://doi.org/10.1002/jbm.a.31587.
[72] Y. Tanimoto, N. Nishiyama, Preparation and physical properties of tricalcium phosphate laminates for bone-tissue engineering, J. Biomed. Mater. Res. A. 85A (2008) 427–433. https://doi.org/10.1002/jbm.a.31569.
[73] A. Shahbaz, M. Abbasi, H. Sabet, Effect of microstructure on mechanical, electrochemical, and biological properties of Ti/HA surface composites fabricated by FSP method, Mater. Today Commun. 37 (2023) 107305. https://doi.org/10.1016/j.mtcomm.2023.107305.
[74] C. Wu, J. Chang, A review of bioactive silicate ceramics, Biomed. Mater. 8 (2013) 032001. https://doi.org/10.1088/1748-6041/8/3/032001.
[75] W. Zhai, H. Lu, C. Wu, L. Chen, X. Lin, et al., Stimulatory effects of the ionic products from Ca–Mg–Si bioceramics on both osteogenesis and angiogenesis in vitro, Acta Biomater. 9 (2013) 8004–8014. https://doi.org/10.1016/j.actbio.2013.04.024.
[76] X. Dong, A. Heidari, A. Mansouri, W.S. Hao, M. Dehghani, et al., Investigation of the mechanical properties of a bony scaffold for comminuted distal radial fractures: Addition of akermanite nanoparticles and using a freeze-drying technique, J. Mech. Behav. Biomed. Mater. 121 (2021) 104643. https://doi.org/10.1016/j.jmbbm.2021.104643.
[77] X. Ke, L. Zhang, X. Yang, J. Wang, C. Zhuang, et al., Low-melt bioactive glass-reinforced 3D printing akermanite porous cages with highly improved mechanical properties for lumbar spinal fusion, J. Tissue Eng. Regen. Med. 12 (2018) 1149–1162. https://doi.org/10.1002/term.2624.
[78] N.E. Putra, M.A. Leeflang, M. Klimopoulou, J. Dong, P. Taheri, et al., Extrusion-based 3D printing of biodegradable, osteogenic, paramagnetic, and porous FeMn-akermanite bone substitutes, Acta Biomater. 162 (2023) 182–198. https://doi.org/10.1016/j.actbio.2023.03.033.
[79] X. Zhang, O. Malekahmadi, S. Mohammad Sajadi, Z. Li, N.H. Abu-Hamdeh, et al., Thermomechanical properties of coated PLA-3D-printed orthopedic plate with PCL/Akermanite nano-fibers: Experimental procedure and AI optimization, J. Mater. Res. Technol. 27 (2023) 1307–1316. https://doi.org/10.1016/j.jmrt.2023.09.215.
[80] X. Wang, Y. Liu, M. Zhang, D. Zhai, Y. Wang, et al., 3D Printing of Black Bioceramic Scaffolds with Micro/Nanostructure for Bone Tumor-Induced Tissue Therapy, Adv. Healthc. Mater. 10 (2021) 2101181. https://doi.org/10.1002/adhm.202101181.
[81] C. Zhao, A. Shen, L. Zhang, K. Lin, X. Wang, Borocarbonitrides nanosheets engineered 3D-printed scaffolds for integrated strategy of osteosarcoma therapy and bone regeneration, Chem. Eng. J. 401 (2020) 125989. https://doi.org/10.1016/j.cej.2020.125989.
[82] X. Li, H. Zhang, H. Zhang, Fabrication of β-TCP/ Akermanite composite scaffold via DLP and in-situ modification of micro-nano surface morphology for bone repair, Ceram. Int. 50 (2024) 2659–2669. https://doi.org/10.1016/j.ceramint.2023.10.276.
[83] N.E. Putra, K.G.N. Borg, P.J. Diaz-Payno, M.A. Leeflang, M. Klimopoulou, et al., Additive manufacturing of bioactive and biodegradable porous iron-akermanite composites for bone regeneration, Acta Biomater. 148 (2022) 355–373. https://doi.org/10.1016/j.actbio.2022.06.009.
[84] C.-I. Dobriţa, A.-I. Bădănoiu, G. Voicu, A.-I. Nicoară, S.-M. Dumitru, et al., Porous bioceramic scaffolds based on akermanite obtained by 3D printing for bone tissue engineering, Ceram. Int. 49 (2023) 35898–35906. https://doi.org/10.1016/j.ceramint.2023.08.270.
[85] A. Nadi, M. Khodaei, M. Javdani, S.A. Mirzaei, M. Soleimannejad, et al., Fabrication of functional and nano-biocomposite scaffolds using strontium-doped bredigite nanoparticles/polycaprolactone/poly lactic acid via 3D printing for bone regeneration, Int. J. Biolog. Macromol. 219 (2022) 1319–1336. https://doi.org/10.1016/j.ijbiomac.2022.08.136.
[86] C. Deng, R. Lin, M. Zhang, C. Qin, Q. Yao, et al., Micro/Nanometer-Structured Scaffolds for Regeneration of Both Cartilage and Subchondral Bone, Adv. Funct. Mater. 29 (2019) 1806068. https://doi.org/10.1002/adfm.201806068.
[87] S. Sahmani, A. Khandan, S. Saber-Samandari, M.M. Aghdam, Vibrations of beam-type implants made of 3D printed bredigite-magnetite bio-nanocomposite scaffolds under axial compression: Application, communication and simulation, Ceram. Int. 44 (2018) 11282–11291. https://doi.org/10.1016/j.ceramint.2018.03.173.
[88] J. Wu, C. Jiao, H. Yu, H. Liang, J. Zhao, et al., A tailored hydroxyapatite/magnesium silicate 3D composite scaffold: Mechanical, degradation, and bioactivity properties, Ceram. Int. 49 (2023) 35438–35447. https://doi.org/10.1016/j.ceramint.2023.08.221.
[89] H. Elsayed, A. Zocca, J. Schmidt, J. Günster, P. Colombo, E. Bernardo, Bioactive glass-ceramic scaffolds by additive manufacturing and sinter-crystallization of fine glass powders, J. Mater. Res. 33 (2018) 1960–1971. https://doi.org/10.1557/jmr.2018.120.
[90] D. He, C. Zhuang, S. Xu, X. Ke, X. Yang, et al., 3D printing of Mg-substituted wollastonite reinforcing diopside porous bioceramics with enhanced mechanical and biological performances, Bioact. Mater. 1 (2016) 85–92. https://doi.org/10.1016/j.bioactmat.2016.08.001.